Using reliability diagrams to interpret the 'signal-to-noise paradox' in seasonal forecasts of the winter North Atlantic Oscilation

Kristian Strommen[1], Molly MacRae[2]and Hannah Christensen[1]

[1]Department of Physics, University of Oxford, UK
[2]Centre for Environmental Data Analysis, UK

Key Points:

- Reliability diagrams for seasonal winter NAO hindcasts are computed and shown to exhibit slopes exceeding 1.
- It is shown that this is equivalent to the RPC value exceeding 1 assuming linearity/Gaussianity of the forecast variable.
- The value of reliability diagrams as a diagnostic tool in seasonal forecasts is discussed.

Corresponding author: Kristian Strommen, kristian.strommen@physics.ox.ac.uk

Abstract

The 'signal-to-noise paradox' for seasonal forecasts of the winter NAO is often described as an 'underconfident' forecast and measured using the ratio-of-predictable components metric (RPC). However, comparison of RPC with other measures of forecast confidence, such as spread-error ratios, can give conflicting impressions, challenging this informal description. We show, using a linear statistical model, that the 'paradox' is equivalent to a situation where the reliability diagram of any percentile forecast has a slope exceeding 1. The relationship with spread-error ratios is shown to be far less direct. We furthermore compute reliability diagrams of winter NAO forecasts using seasonal hindcasts from the European Centre for Medium-range Weather Forecasts and the UK Meteorological Office. While these broadly exhibit slopes exceeding 1, there is evidence of asymmetry between upper and lower terciles, indicating a potential violation of linearity/Gaussianity. The limitations and benefits of reliability diagrams as a diagnostic tool are discussed.

Plain Language Summary

The North Atlantic Oscillation (NAO) is an atmospheric phenomenon which can be understood as summarising large-scale winter conditions across western Europe. Long-range forecasts of the NAO have been shown to be skillful, but also to suffer from a so-called 'signal-to-noise paradox', which roughly says that the real world appears to be more predictable than the forecasts think it is. However, interpreting the exact meaning of this 'paradox' has proved challenging. We help bring some clarity by showing that one can interpret the 'paradox' as a case of a probabilistically underconfident forecast, namely a forecast which tends to underestimate the likelihood of high magnitude NAO events.

1 Introduction

It is now well established that weather forecasting models are able to generate skillful seasonal forecasts of the winter North Atlantic Oscillation (NAO) (Smith et al., 2016; Eade et al., 2014; Dunstone et al., 2016; Athanasiadis et al., 2017). However, these forecasts also suffer from a curious phenomenon dubbed a 'signal-to-noise paradox' (Eade et al., 2014; Dunstone et al., 2016). An overview and discussion of this phenomenon is given by Scaife and Smith (2018), who also explain why understanding, and ultimately eliminating the 'paradox' from forecasts is a problem of great practical importance.

The 'paradox' is commonly measured using a correlation based metric referred to as the 'ratio-of-predictable components' (RPC), as introduced in Eade et al. (2014). A forecast is said to exhibit a 'signal-to-noise paradox' when RPC > 1, which corresponds to a situation where the ensemble mean is a better predictor of the real world than of individual ensemble members (see Section 2.4). However, interpreting this situation and understanding how RPC relates to other skill metrics has proved challenging. Indeed, the choice of the word 'paradox' suggests that this phenomenon is often viewed as strange and unintuitive by the weather forecasting community. Eade et al. (2014) interpreted forecasts with RPC > 1 as being 'underconfident', but in Strommen and Palmer (2019) it was shown that root-mean square spread-error ratios, another metric widely used to measure forecast confidence (Johnson & Bowler, 2009), do not always give the same qualitative conclusion as the RPC. In fact, one can easily construct statistical forecast models that are 'underconfident' with respect to RPC but 'overconfident' with respect to RMS spread-error (Strommen & Palmer, 2019), and there is evidence suggesting such a mismatch actually occurs in the case of winter NAO forecasts (A. Weisheimer et al., 2019). Given these subtleties, it seems valuable to further our understanding about what exactly the 'paradox' is measuring.

The goal of the present paper is to address the following questions:

1. Can reliability diagrams (Murphy, 1973), which measure probabilistic forecast skill, be used to measure the 'signal-to-noise paradox', and if yes, what is the relation between such diagrams and the RPC metric?
2. How reliable are seasonal winter NAO forecasts, as measured by computing reliability diagrams of two state-of-the-art forecast models?

The value of reliability diagrams as a tool to study seasonal forecasts was first highlighted by A. Weisheimer and Palmer (2014), who emphasised the importance of using genuinely probabilistic metrics when assessing forecast skill. Reliability diagrams offer an intuitive and easy-to-interpret measure of forecast confidence: a forecast of a binary event E can be thought of as 'overconfident' if, in situations where the forecast probability P_f of E occurring is high, event E actually occurs in the real world with a frequency less than P_f. In other words, the forecast model overestimates the true probability of E occurring. Similarly, an 'underconfident' model would be one where the forecast model underestimates the true probability.

To address these questions, we will make use of two types of data. Firstly, we will use artificially generated data based on the simple 'signal plus noise' statistical model of Siegert et al. (2016). This will allow us to assess forecast reliability and its relation to RPC in an idealised situation where, in particular, the sample size can be made large enough to minimise noise. In fact, the explicit nature of the statistical model allow for a theoretical comparison between reliability and RPC. Secondly, we will compute the winter NAO forecast reliability for two world-leading forecast models: the UK Met Office model (UKMO) (Scaife et al., 2014) and the European Centre for Medium-range Weather Forecasts (ECMWF) model (A. Weisheimer et al., 2017).

2 Data and methods

2.1 Data

The UKMO hindcast data used is the 40-member 'DePreSys3' ensemble, based on the HadGEM3-GC2 version of Met Office Unified Model, as described in Dunstone et al. (2016). The dataset consists of 35 ensemble forecasts initialised on November 1st for every year between 1980 and 2015. The forecast model includes interactive atmosphere-ocean coupling and has a nominal atmospheric resolution of 0.83° longitude by 0.55° latitude with 85 vertical levels. The nominal ocean resolution is 0.25°. The ensemble mean NAO correlations attained are approximately 0.6.

The ECMWF data used is the 51-member ensemble 'ASF20C', based on a version of the Integrated Forecast System (IFS) closely related to the System 4 forecast system (Molteni et al., 2011). ASF20C consists of 110 ensemble forecasts initialised on November 1st for every year between 1900 and 2010. The horizontal spectral resolution of the model of T255 corresponds to a grid length of approximately 80 km with 91 vertical levels. ASF20C is uncoupled, and uses prescribed SSTs from the ERA20C reanalysis (Poli et al., 2016). Further details can be found in A. Weisheimer et al. (2017). The ensemble mean NAO correlations attained over the period 1980-2010 are approximately 0.5.

We use ERA20C as our observational 'truth' in order to allow for a comparison with ASF20C across the whole 20th century. In order to have a clean comparison with the UKMO data, we will consider the 31 winters covering 1980-2010 ($N = 31$), as well as the full period 1900-2010 ($N = 109$). We only work with DJF means, with each DJF season labelled according to the year of the corresponding January.

2.2 Definition of the NAO index

The NAO timeseries for ERA20C and all ECMWF/UKMO ensemble members are defined as in Dunstone et al. (2016), namely as the difference in DJF-averaged mean sea-level pressure anomalies between Iceland (63-70N, 25-16W) and the Azores (36-40N, 28-20W). The timeseries are normalised to have mean 0 and standard deviation 1.

2.3 Reliability diagrams and definition of the forecast events

There are a wealth of resources and prior literature concerning reliability diagrams (Murphy & Winkler, 1977; Bröcker & Smith, 2007; A. Weisheimer & Palmer, 2014). For completeness we provide the basic definitions.

Suppose we have an ensemble forecast of a binary event E at times t consisting of ensemble members $x_{t,k}, k = 1, \dots R$, where R is the ensemble size. Let y_t be the timeseries of E as observed in the real world. At time t, the forecast probability P_f of E occurring is defined as the proportion of ensemble members for which E occurs. By considering all times t that share approximately the same forecast probability P_f, we can compute the proportion P_r of such times in which y_t registered an occurrence of E. A reliability diagram is simply a plot of P_f against P_r.

A reliable forecast is one where $P_f = P_r$, which is guaranteed for a perfectly calibrated ensemble. In this case the reliability diagram coincides with the diagonal and the slope of a linear fit to the data will be 1. A forecast is said to be unreliable if the reliability diagram deviates from the diagonal. We therefore obtain a quantitative measure of the reliability of a forecast by estimating the slope of the reliability diagram. This measure is only sensible in cases where the relationship between P_f and P_r is approximately linear. Reliability diagrams computed using weather forecast data can often deviate strongly from linearity, but we will see that in our case the assumption of linearity is reasonable.

When applying this framework to seasonal NAO forecasts we follow standard conventions by defining two binary events in terms of the upper and lower tercile of the distribution. These events can jointly be thought of as assessing the reliability of forecasts predicting a notable deviation from neutral conditions. The forecast (observed) probability is computed with respect to the terciles of the forecast (observational) distribution, to avoid overpenalising.

Probability/occurrence bins are defined for each decile (0-10%, 10-20%, etc.). When fitting a straight line to the raw scatter plot, the bins are weighted according to the number of samples they contain.

2.4 Statistical testing and the RPC metric

For significance tests, we use Monte Carlo resampling: generate 1000 random samples, compute the relevant metric in all 1000 cases, and use the resulting distribution to generate confidence intervals. With the SN-model, random pairs of 'observations' and 'forecasts' are generated by taking random draws from the distributions of s, ϵ and η and using the SN-model equations. When considering UKMO/ECMWF forecast data, random draws are generated by resampling years randomly with replacement to obtain shuffled timeseries of the same length as the original.

The RPC metric is defined by the formula

$$RPC = \frac{\sqrt{Corr(EnsMean, Obs)^2}}{\sqrt{\sigma_{sig}^2/\sigma_{tot}^2}}, \tag{1}$$

where $EnsMean$ is the ensemble mean timeseries, Obs is the observational timeseries, σ^2_{sig} is the ensemble mean variance, σ^2_{tot} is the average variance of individual ensemble members, and the square root is always taken to be positive. Eade et al. (2014) motivate this metric, and its name, by noting that if the forecast has skill, then the RPC is a lower bound approximation to the ratio $PC(Obs)/PC(Mod)$, where the numerator (denominator) is the square root of the proportion of variance that is predictable in the real world (the forecast world). It can be shown (Strommen & Palmer, 2019) that

$$RPC \approx \frac{Corr(EnsMean, Obs)}{Corr(EnsMean, Mem)}, \tag{2}$$

where $Corr(EnsMean, Mem)$ denotes the average correlation between the ensemble mean and individual ensemble members. Thus RPC $>$ 1 can be understood as a situation where the ensemble mean correlates better with the real world than with random members, which in turn implies that the forecast underestimates the predictability of the real world. Equation (2) makes it clear that for a statistically perfect forecast (one where observations are indistinguishable from a random ensemble member), $RPC = 1$. Further discussion on RPC can be found in Scaife and Smith (2018) and Strommen and Palmer (2019).

2.5 The 'signal-plus-noise' statistical model

We use the idealised statistical model defined in Siegert et al. (2016), which they refer to as a signal-plus-noise model, and which we will refer to as the SN-model for short. It assumes the forecast signals are linear and Gaussian. The reader should refer to their paper for extensive discussion. Here we simply recap the basic details we need.

Let y_t be the NAO index of the real world, and $x_{t,k}, k = 1, \dots R$ be the NAO indices of an ensemble forecast of y with R members. If the NAO indices have been defined or normalised so as to have zero mean, the SN-model supposes that

$$\begin{aligned} y_t &= s_t + \epsilon_t \\ x_{t,k} &= \beta s_t + \eta_t. \end{aligned}$$

Here s_t, ϵ_t and η_t are all independent, normally distributed variables with mean zero and standard deviations $\sigma_s, \sigma_\epsilon, \sigma_\eta$, and β is a constant representing the sensitivity of the forecasts to the observations. One can interpret this as decomposing the observed NAO y_t into a predictable signal s_t, and an unpredictable noise term ϵ_t. The forecast attains skill by capturing a proportion βs_t of s_t, and has its own noise given by η_t. The ensemble members are assumed to be completely exchangeable with each other, exhibiting both the same signal and same level of noise.

It will be useful to note that the independence assumptions imply that $Var(y) = \sigma_s^2 + \sigma_\epsilon^2$ and $Var(x) = \beta^2\sigma_s^2 + \sigma_\eta^2$. Siegert et al. (2016) also derive a formula for the RPC of the SN-model in their Appendix B, which in the limit of infinitely many ensemble members becomes

$$RPC_{SN} = \frac{1}{\beta}\frac{\sqrt{\beta^2\sigma_s^2 + \sigma_\eta^2}}{\sqrt{\sigma_s^2 + \sigma_\epsilon^2}}. \tag{3}$$

Thus RPC > 1 occurs in this model as a result of either a small signal ($\beta < 1$) or excessive forecast variance (which when $\beta = 1$ happens if $\sigma_\eta > \sigma_\epsilon$).

To compare the forecast data to the SN-model behaviour, we fit the free parameters of the SN-model to UKMO and ECMWF forecast data. To do so, we used the 'moment estimator method' described in Appendix C of Siegert et al. (2016). The estimated values of $(\sigma_s, \sigma_\epsilon, \sigma_\eta, \beta)$ are $(0.79, 0.61, 0.99, 0.27)$ for UKMO data, and $(0.60, 0.80, 0.98, 0.37)$ for ECMWF data. These values will be discussed in Section 4.1. Because this discussion is not central to the paper, error-bars are omitted, but one can infer from the un-

certainty estimates in Siegert et al. (2016) that the differences between UKMO and ECMWF parameters are likely not statistically significant.

3 Results using the idealised statistical model

3.1 Numerical analysis

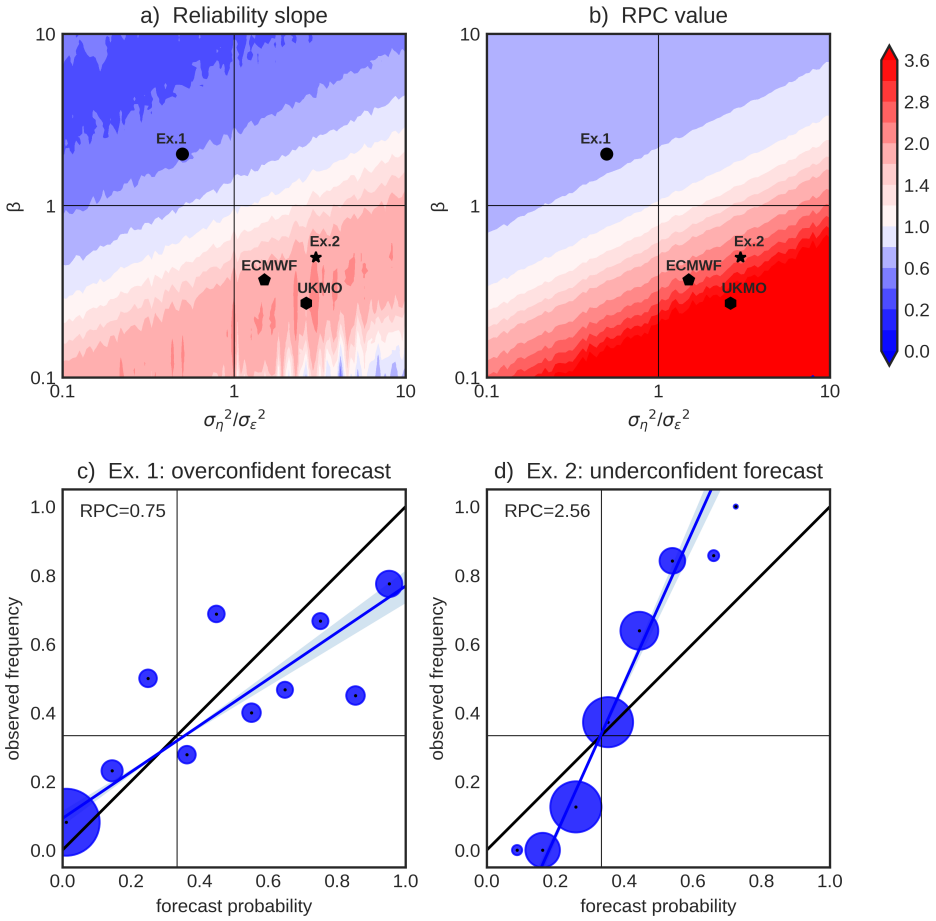

Figure 1. Reliability and RPC estimates using the SN-model. In (a) a contour plot of the slope of the reliability diagram across a range of SN-model parameters. In (b) the same but for RPC. In (c) and (d): example reliability diagrams obtained for a specific choice of parameters corresponding to an overconfident and underconfident forecast respectively. The sizes of the blue dots are proportional to the number of samples available in that bin; the blue line is the linear fit and the blue shading gives the 95% confidence interval of this linear fit. In (a) and (b), the location of the two examples (black dot and star) as well as the UKMO and ECMWF fits (black hexagon and pentagon) have been marked.

In order to understand how reliability relates to RPC in the SN-model, we proceed as follows. We first fix the 'observational' parameters σ_s and σ_ϵ to be the UKMO estimates from Section 2.5. We then pick random values of the 'forecast' parameters β and σ_η uniformly between 0.10 and 10. These parameters are used to generate an observational timeseries y and 50 ensemble member timeseries x_k, each of length $N = 1000$. For each such pair of observations and ensemble, we compute the slope of reliability di-

agrams corresponding to the upper and lower tercile events, along with the RPC value. The large sample size of 1000 reduces the sampling variability and helps highlight general patterns. Figure 1(a) and (b) show how these metrics vary as a function of both β and $\sigma_\eta^2/\sigma_\epsilon^2$ in the case of the upper tercile event. Note that because the SN-model is linear, reliability diagrams for upper and lower terciles are always identical. Large (small) values of β are interpreted as the signal being large (small) in the forecast, while large (small) values of $\sigma_\eta^2/\sigma_\epsilon^2$ are interpreted as the forecast members exhibiting more (less) unpredictable noise than the real world. We refer to this latter ratio as the noise-ratio for short.

Several points can be inferred from Figure 1. Firstly, it can be seen that the reliability of the slope varies monotonically with both β and the noise-ratio. Three essential parameter regimes can be identified, corresponding to the value of the slope S: $S < 1$ (overconfident), $S > 1$ (underconfident) and $S = 1$ (perfect reliability). An example reliability diagram from the $S < 1$ regime is shown in Figure 1(c) ($\beta = 2, \sigma_\eta = \sigma_\epsilon/2$) , and an example for the $S > 1$ regime in Figure 1(d) ($\beta = 0.5, \sigma_\eta = 2\sigma_\epsilon$). In order for the forecast model to be perfectly statistically calibrated, it is necessary for both β and the noise-ratio to be 1. However, Figure 1(a) shows that perfect reliability can be obtained for a non-perfect forecast model through a compensation of errors: too much (little) noise can be balanced by an overly strong (weak) signal, and vice versa. This explains why the $S = 1$ regime sits on the diagonal.

Secondly, comparing Figures 1(a) and (b) strongly suggests that the parameter regimes defined by $RPC < 1$, $RPC > 1$ ('paradox') and $RPC = 1$ are *the same* as those defined using the reliability slope. In other words, the model parameters that lead to a reliability slope $S > 1$ are the same parameters that give $RPC > 1$. In fact, in the next section we will prove this statement under the assumptions of a sufficiently large sample and ensemble size. This means that in the SN-model, the 'paradox' can be precisely understood as an instance of a forecast with reliability slope $S > 1$.

A final point of note concerns the impact of sampling variability. The artefacts in the contour of Figure 1(a) suggest that sampling variability remains non-trivial even with a sample size of $N = 1000$. This can be seen in the two example diagrams (c) and (d), showing deviations from linearity that are necessarily due to sampling variability alone. The effect is especially big in the bottom right corner of Figure 1(a), corresponding to the limiting case where ensemble members are purely noise-driven, implying that reliability cannot be sensibly assessed unless the forecast has sufficient skill. By comparison with Figure 1(b), the sample size of 1000 appears sufficient to eliminate sampling variability for RPC estimates, even in the noise-driven limit case. However, in regions closer to the diagonal, the sampling variability of the reliability slope is small enough to easily assess which parameter-regime one is in.

3.2 Theoretical analysis

We sketch a proof of the equivalence $S > 1 \iff RPC > 1$ in the SN-model, under the assumption that (a) the ensemble size is large enough that the ensemble mean $\hat{x}_t \approx \beta s_t$ (i.e., noise is completely eliminated), and (b) the sample size is large enough that sample estimates (of e.g. variances) equal the true underlying population values. For simplicity we also assume $\beta > 0$, i.e. that the forecasts have non-zero skill. The sketch assumes the event definition E is the upper tercile: at the end we indicate why the same argument accounts for an arbitrary upper/lower percentile.

It is possible to derive exact formulae for the reliability curve (i.e. P_r as a function of P_f) which show that the curve is a strictly increasing 'sigmoid' whose growth rate is determined by the RPC. These formulae exhibit degeneracies when the ensemble mean correlation is very close to 1, which in the SN-model happens when $\sigma_s >> \sigma_\epsilon$. The sketch

which follows is essentially correct away from this region and captures the key ideas. Complete details can be found in the Supporting Information.

First note that given the assumption that ensemble mean correlations are not close to 1, the reliability curve will approximately pass through the point $(1/3, 1/3)$. Intuitively, a forecast probability of $1/3$ corresponds to a forecast which detects no appreciable predictable signal and which therefore gives us no knowledge about the value of y_t. Consequently, y_t is roughly speaking expected to be a random draw from its climatology, which lands in the upper tercile with probability $1/3$, as desired.

Next, we will show that $RPC > 1$ if and only if the reliability curve passes through the point $(1/2, L)$ for some $L > 1/2$, i.e. a point above the diagonal. By definition, $L = \mathbb{P}(y_t \text{ satisfies } E \mid P_f = 0.5)$, where P_f is the forecast probability. Because y_t is normally distributed with variance $\sigma_s^2+\sigma_\epsilon^2$, its upper tercile is defined by $y_t > \lambda\sqrt{\sigma_s^2 + \sigma_\epsilon^2}$, where $\lambda \approx 0.431$ defines the upper tercile threshold of the $\mathcal{N}(0, 1)$ distribution. Similarly, the upper tercile for the forecast distribution is defined by $x_{t,k} > \lambda\sqrt{\beta^2\sigma_s^2 + \sigma_\eta^2}$. Since ensemble members are normally distributed around the ensemble mean, $P_f = 0.5$ if and only if half the members exceed the upper tercile threshold, which happens if and only if the ensemble mean βs_t *equals* the forecast upper tercile threshold. Therefore,

$$L = \mathbb{P}\left(y_t = s_t + \epsilon_t > \lambda\sqrt{\sigma_s^2 + \sigma_\epsilon^2} \mid \beta s_t = \lambda\sqrt{\beta^2\sigma_s^2 + \sigma_\eta^2}\right). \tag{4}$$

This is the probability of ϵ_t exceeding a fixed threshold conditioned on the value of s_t. Since ϵ and s are independent, the conditional can be dropped, yielding

$$L = \mathbb{P}\left(\epsilon_t > \lambda\sqrt{\sigma_s^2 + \sigma_\epsilon^2} - \frac{\lambda}{\beta}\sqrt{\beta^2\sigma_s^2 + \sigma_\eta^2}\right). \tag{5}$$

Because ϵ_t is normally distributed with mean 0, this probability exceeds 0.5 if and only if the right-hand-side of the inequality in (5) is less than 0. Rearranging and simplifying this implies

$$L > 0.5 \iff \frac{\sqrt{\beta^2\sigma_s^2 + \sigma_\eta^2}}{\beta\sqrt{\sigma_s^2 + \sigma_\epsilon^2}} > 1, \tag{6}$$

which by equation 3 precisely says that RPC > 1.

We have shown that the reliability curve intersects the diagonal at $P_f = 1/3$ and is above the diagonal at $P_f = 1/2 \iff RPC > 1$. Since the reliability curve is strictly increasing, this already clarifies why $S > 1 \iff RPC > 1$. Similar arguments show that the curve is always below the diagonal for $P_f < 1/3$ and always above the diagonal for $P_f > 1/2$. The explicit sigmoid shape of the curve can be used to guarantee an overall slope exceeding 1, finishing the proof sketch.

The case where E is the lower tercile only requires a slight modification: the lower terciles are defined by the condition of being less than $-\lambda$ times the variance. The reversing of the inequality and the change of the sign cancel out in the end to give the same conclusion. If a different percentile C had been used to define E, then as long as $C < 0.5$ the exact same argument will work. If $C > 0.5$, the same argument can be applied to the lower percentile event $1 - C$ to establish the same claim by symmetry.

It is interesting to note that an expression for the root mean-squared-error divided by the average ensemble spread can also be established under the same assumptions of large sample and ensemble size:

$$\frac{\text{RMSE}}{\text{Spread}} = \frac{\sqrt{(\beta-1)^2\sigma_s^2 + \sigma_\epsilon^2}}{\sigma_\eta},$$

where the precise meaning of RMSE and Spread are as in Fortin et al. (2014). Given a statistically perfect forecast this ratio equals 1 (Fortin et al., 2014), which can be easily verified in our case by setting $\beta = 1$ and $\sigma_\epsilon = \sigma_\eta$, the conditions required for perfect statistical calibration (Siegert et al., 2016). However, it is clear that for a non-perfect forecast, the relationship between this ratio and RPC (or the reliability slope) is not straightforward, suggesting that spread-error metrics are measuring forecast confidence in a fundamentally different manner to RPC and reliability diagrams.

4 Results using forecast data

We consider in turn the modern period 1980-2010 and the full period 1900-2010. Note that a full discussion of the challenges arising from sampling variability is reserved for Section 5.

4.1 The period 1980-2010

Figure 2 shows the reliability diagrams of seasonal winter NAO forecasts using both the upper and lower tercile events, for ECMWF and UKMO forecast data, using the period 1980-2010 ($N = 31$) for which they overlap. Thick red lines show the raw estimate, with shading indicating uncertainty.

In diagrams (a), (c) and (d), the NAO reliability slope exceeds 1, and robustly so for the upper tercile event. In (b), the lower tercile event for ECMWF, the uncertainty is too great to assess the reliability, but the overall assessment of both NAO forecasts is that they are unreliable and underconfident. Given the conclusions of the previous section, this is consistent with the presence of the 'signal-to-noise paradox' of these forecasts, with the UKMO and ECMWF exhibiting an RPC of 2.3 and 1.8 respectively. Therefore, despite the large uncertainties in the exact quantitative estimates of several of the reliability slopes in Figure 2, these diagrams give the same qualitative conclusion as analysis based on RPC.

The equivalence of reliability and RPC in the previous section assumed the linear and Gaussian SN-model. The only indication of a violating of linearity/Gaussianity here is in the discrepancy being between the upper and lower ECWMF terciles. However, the uncertainty of the lower tercile slope is large enough to still be consistent with the SN-model.

In order to allow for a qualitative comparison between UKMO and ECMWF, their positions in $(\beta, \sigma_\eta^2/\sigma_\epsilon^2)$-space have been marked on Figures 1(a) and (b), though we remind the reader that the uncertainty in the parameters means this comparison should be treated cautiously. The ECMWF forecasts appear to be slightly more reliable than UKMO, exhibiting both a higher β and a noise-ratio closer to 1. However, this is at the expense of less skill than UKMO, due to a smaller overall signal σ_s. The differing values of σ_s and σ_ϵ for the two datasets (Section 2.5) may seem puzzling, given the same observations are used for each. However, as emphasised in Siegert et al. (2016), the decomposition of observations into s and ϵ is a statistical construct which is in no way independent of the forecast product being used. For example, if UKMO simulates a teleconnection missing in ECMWF, a parameter fit using UKMO will assign the variability associated with this teleconnection to the signal, while ECMWF would assign it to the noise.

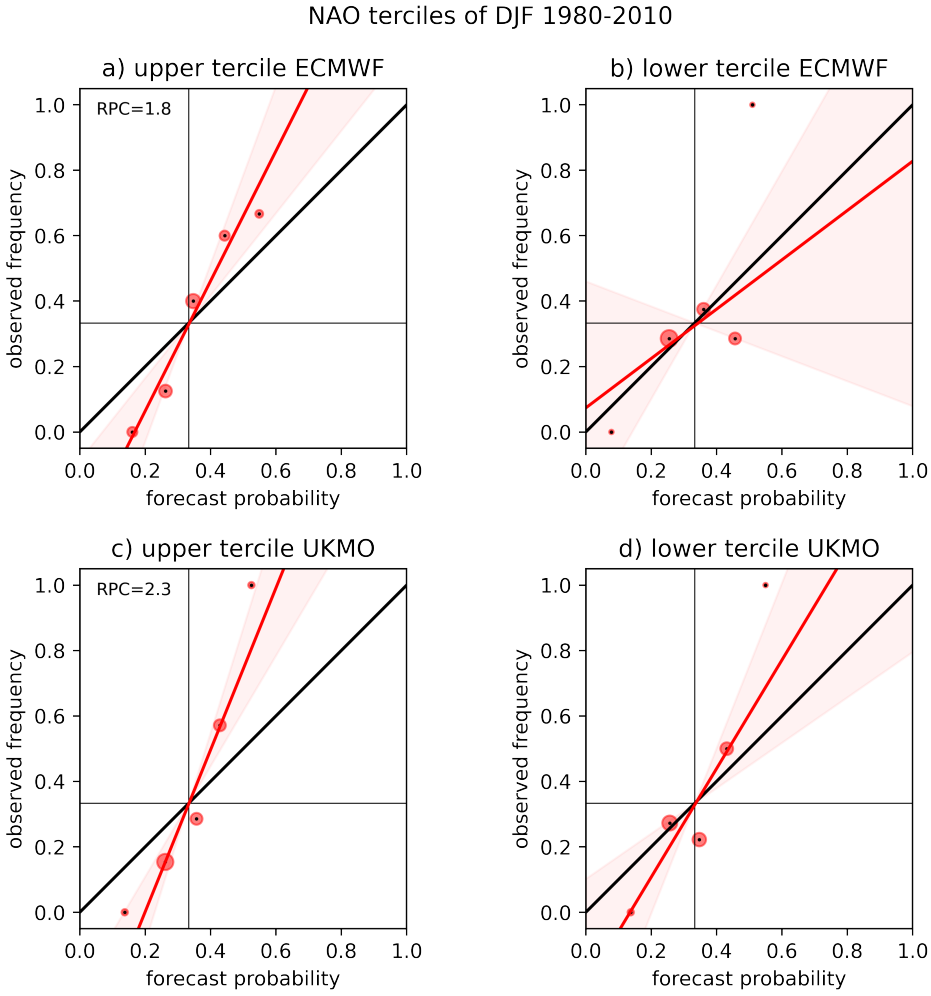

Figure 2. In (a) and (b), reliability diagrams of, respectively, upper and lower tercile DJF NAO forecasts by the ECMWF ensemble, and in (c) and (d) the same but for UKMO forecasts. The period covered is 1980-2010. The sizes of the red dots are proportional to the number of samples available in that bin; the thick red line is the linear fit and the red shading gives the 95% confidence interval of this linear fit. The 'perfect reliability' diagonal (thick black line) is included for convenience.

4.2 The period 1901-2010

Figure 3 shows the reliability diagrams for the ECMWF model covering the full 110-year period 1901-2010 ($N = 109$). While the upper tercile uncertainty crosses the diagonal, the face-value reliability slope indicates underconfidence, consistent with the modern period 1980-2010. On the other hand, the lower tercile interestingly indicates robust *overconfidence*, giving an overall impression of good reliability when considering both terciles jointly.

These results are consistent with the analysis in A. Weisheimer et al. (2019), which showed that RPC ≈ 1 in these forecasts when computed over the period 1901-2010. Their analysis further showed pronounced decadal variability in both skill and RPC, with the modern period standing out as an era of relatively high skill and RPC values. These re-

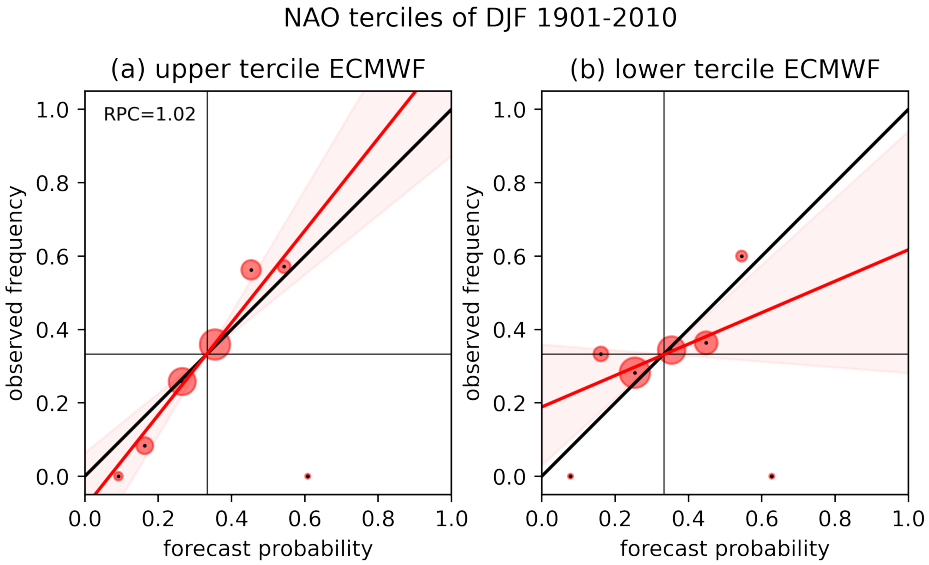

Figure 3. In (a) and (b), reliability diagrams of, respectively, upper and lower tercile DJF NAO forecasts by the ECMWF ensemble. The period covered is 1901-2010. The sizes of the red dots are proportional to the number of samples available in that bin; the thick red line is the linear fit and the red shading gives the 95% confidence interval of this linear fit. The 'perfect reliability' diagonal (thick black line) is included for convenience.

liability diagrams, if taken at face value, complement A. Weisheimer et al. (2019) by indicating that the main source of both skill and high RPC values are forecasts of positive NAO events, with forecasts of negative events being qualitatively different. In particular, the ECMWF underconfidence of positive NAO events and overconfidence of negative NAO events appear to be relatively consistent features across both the full period 1901-2010 and the modern period 1980-2010.

5 Discussion and conclusions

We have shown, given the assumption of linearity/Gaussianity, that the 'signal-to-noise paradox' corresponds precisely to a situation where upper/lower percentile forecasts have a reliability diagram with a slope exceeding 1. More precisely, by utilising the linear statistical model of Siegert et al. (2016), we showed that given a large sample size and sufficiently many ensemble members, the RPC metric exceeds 1 if and only if the reliability slope exceeds 1: the higher the RPC, the steeper the slope, and vice versa. This justifies the intuitive interpretation of the 'paradox' as a case of an 'underconfident forecast', with confidence measured probabilistically using reliability diagrams. On the other hand, the ratio of RMSE over ensemble spread is not straightforwardly related to RPC, meaning that this interpretation does not hold if confidence is measured using spread-error ratios.

Furthermore, we showed, using ECMWF and UKMO seasonal hindcasts, that tercile forecasts of the winter NAO generally exhibit reliability diagrams with slopes exceeding 1. In other words, the 'signal-to-noise paradox' present in these hindcasts can be detected using reliability diagrams. Consideration of the ECMWF hindcast, which covers the full 20th century, suggests that the main source of forecast underconfidence is from positive NAO forecasts, with negative NAO forecasts being more overconfident on av-

erage. This apparent asymmetry between positive and negative NAO forecasts indicates a violation of linearity/Gaussianity, which may be due to the effects of skew (Stephenson et al., 2004), flow-dependent predictability (Frame et al., 2013; Ferranti et al., 2015; Matsueda & Palmer, 2018), or non-linear regime dynamics (Strommen, 2020). The relationship with A. Weisheimer et al. (2017), which found that ECMWF skill is higher for negative NAO events, is unclear, since higher skill might be expected to increase the RPC (by equation 2) and hence lead to underconfidence. The asymmetry may also be a random artefact.

The clear limitation to the use of reliability diagrams to assess seasonal mean forecasts, such as the winter NAO, is the uncertainty arising from sampling variability. This uncertainty has two sources. Firstly, given the 1980-2010 hindcast sample size of 31, each forecast-probability bin was found to contain somewhere between 3 and 10 samples, which is clearly insufficient to robustly estimate the conditional observed frequency. Secondly, the 'paradox' has the effect of clustering forecast probabilities close to 50%, meaning there are few cases of extreme forecast probabilities available, especially high-probability cases. The resulting uncertainty means that reliability diagrams based on a typical hindcast sample size of 30-40 years can only sensibly be used for qualitative, rather than quantitative, assessment. Longer hindcasts spanning the 20th century currently only exist for the ECMWF model.

The fact that reliability diagrams are particularly sensitive to sampling variability is well known, and several 'tactics' have become standard for overcoming this. For example, when assessing reliability of seasonal forecasts for a particular region (such as the UK), it is common to treat forecasts for each individual gridpoint in the region as independent instances of the regional forecast (A. Weisheimer & Palmer, 2014). While this has the effect of dramatically increasing the sample size, the assumptions will clearly often fail: neighboring gridpoints are not independent and the presence of orography means individual gridpoints may not be representative of the region as a whole. The large uncertainties in the 1980-2010 winter NAO reliability estimates (Figure 2) may seem less unfavourable in this light. We also note that uncertainties in RPC estimation are typically considerable: in cases of low forecast skill (ensemble mean correlations < 0.4) these uncertainties can easily be large enough to make it impossible to assess if the RPC is greater or less than 1 (Strommen & Palmer, 2019).

Nevertheless, it is natural to ask if tactics similar to the use of gridpoint forecasts can be used to more robustly assess the reliability of winter NAO forecasts. One possibility is to use forecasts of the December, January and February NAO separately. This was explored, but found to pose challenges, since forecast skill was found to not be uniform across each month, with December showing little to no skill. It is therefore not immediately clear how to relate reliability of the pooled monthly forecasts to reliability of the seasonal mean forecast. Other future avenues of exploration might include pooling forecasts of multiple principal components beyond just the first.

In conclusion, despite the limitations imposed by sampling variability, we propose that reliability diagrams of seasonal means can provide a useful complementary view of the 'signal-to-noise paradox', and more broadly contribute to the qualitative assessment of seasonal forecasts. In particular, exploration of both upper and lower percentile forecasts seems valuable as an easy way to help identify the largest contributors to the 'paradox' in a way that the raw RPC cannot. The theoretical relationship between RPC and reliability slopes we established is also helpful for guiding intuition. It would be interesting to assess if a similar relationship holds in more non-linear models, such as the regime-based one of Strommen and Palmer (2019).

6 Open Research

The NAO hindcast timeseries and python code used to create the figures of this paper are freely available on GitHub: `https://github.com/KristianJS/reliability_diags/`

ASF20C data is freely available on CEDA (C. Weisheimer A.; O'Reilly, 2020). ERA20C data is freely available via ECMWF at `https://apps.ecmwf.int/datasets/data/era20c-daily/levtype=sfc/type=an/`.

Acknowledgments

KS gratefully acknowledges funding from the Thomas Philips and Jocelyn Keene Junior Research Fellowship, Jesus College. MM acknowledges funding from the Met Office Academic Partnership (MOAP), which funded their work across the summers of 2021 and 2022. HC acknowledges NERC grant NE/P018238/1.

References

Athanasiadis, P. J., Bellucci, A., Scaife, A. A., Hermanson, L., Materia, S., Sanna, A., ... Gualdi, S. (2017). A multisystem view of wintertime NAO seasonal predictions. *Journal of Climate*, *30*(4), 1461–1475.

Bröcker, J., & Smith, L. A. (2007). Increasing the reliability of reliability diagrams. *Weather and forecasting*, *22*(3), 651–661.

Dunstone, N., Smith, D., Scaife, A., Hermanson, L., Eade, R., Robinson, N., ... Knight, J. (2016, oct). Skilful predictions of the winter North Atlantic Oscillation one year ahead. *Nature Geoscience 2016 9:11*, *9*(11), 809–814. doi: 10.1038/ngeo2824

Eade, R., Smith, D., Scaife, A., Wallace, E., Dunstone, N., Hermanson, L., & Robinson, N. (2014, aug). Do seasonal-to-decadal climate predictions underestimate the predictability of the real world? *Geophysical Research Letters*, *41*(15), 5620–5628. doi: 10.1002/2014GL061146

Ferranti, L., Corti, S., & Janousek, M. (2015). Flow-dependent verification of the ECMWF ensemble over the Euro-Atlantic sector. *Quarterly Journal of the Royal Meteorological Society*, *141*(688), 916–924.

Fortin, V., Abaza, M., Anctil, F., & Turcotte, R. (2014). Why should ensemble spread match the rmse of the ensemble mean? *Journal of Hydrometeorology*, *15*(4), 1708–1713.

Frame, T., Methven, J., Gray, S., & Ambaum, M. (2013). Flow-dependent predictability of the North Atlantic jet. *Geophysical Research Letters*, *40*(10), 2411–2416.

Johnson, C., & Bowler, N. (2009). On the reliability and calibration of ensemble forecasts. *Monthly Weather Review*, *137*(5), 1717–1720.

Matsueda, M., & Palmer, T. (2018). Estimates of flow-dependent predictability of wintertime Euro-Atlantic weather regimes in medium-range forecasts. *Quarterly Journal of the Royal Meteorological Society*, *144*(713), 1012–1027.

Molteni, F., Stockdale, T., Balmaseda, M., Balsamo, G., Buizza, R., Ferranti, L., ... Vitart, F. (2011). *The new ECMWF seasonal forecast system (System 4)* (Vol. 49). European Centre for medium-range weather forecasts Reading.

Murphy, A. H. (1973). A new vector partition of the probability score. *Journal of Applied Meteorology and Climatology*, *12*(4), 595–600.

Murphy, A. H., & Winkler, R. L. (1977). Reliability of subjective probability forecasts of precipitation and temperature. *Journal of the Royal Statistical Society: Series C (Applied Statistics)*, *26*(1), 41–47.

Poli, P., Hersbach, H., Dee, D. P., Berrisford, P., Simmons, A. J., Vitart, F., ... Fisher, M. (2016, jun). ERA-20C: An Atmospheric Reanalysis of

455 the Twentieth Century. *Journal of Climate*, *29*(11), 4083–4097. doi:
456 10.1175/JCLI-D-15-0556.1
457 Scaife, A. A., Athanassiadou, M., Andrews, M., Arribas, A., Baldwin, M., Dunstone,
458 N., ... Williams, A. (2014, mar). Predictability of the quasi-biennial oscilla-
459 tion and its northern winter teleconnection on seasonal to decadal timescales.
460 *Geophysical Research Letters*, *41*(5), 1752–1758. doi: 10.1002/2013GL059160
461 Scaife, A. A., & Smith, D. (2018, dec). A signal-to-noise paradox in climate science.
462 *npj Climate and Atmospheric Science*, *1*(1), 28. doi: 10.1038/s41612-018-0038
463 -4
464 Siegert, S., Stephenson, D. B., Sansom, P. G., Scaife, A. A., Eade, R., & Arribas, A.
465 (2016). A Bayesian framework for verification and recalibration of ensemble
466 forecasts: How uncertain is NAO predictability? *Journal of Climate*, *29*(3),
467 995–1012.
468 Smith, D. M., Scaife, A. A., Eade, R., & Knight, J. R. (2016, jan). Seasonal to
469 decadal prediction of the winter North Atlantic Oscillation: emerging capa-
470 bility and future prospects. *Quarterly Journal of the Royal Meteorological*
471 *Society*, *142*(695), 611–617. doi: 10.1002/QJ.2479
472 Stephenson, D. B., Hannachi, A., & O'Neill, A. (2004, jan). On the existence of
473 multiple climate regimes. *Quarterly Journal of the Royal Meteorological Soci-*
474 *ety*, *130*(597), 583–605. doi: 10.1256/QJ.02.146
475 Strommen, K. (2020). Jet latitude regimes and the predictability of the north
476 atlantic oscillation. *Quarterly Journal of the Royal Meteorological Society*,
477 *n/a*(n/a). doi: 10.1002/qj.3796
478 Strommen, K., & Palmer, T. N. (2019, jan). Signal and noise in regime systems:
479 A hypothesis on the predictability of the North Atlantic Oscillation. *Quar-*
480 *terly Journal of the Royal Meteorological Society*, *145*(718), 147–163. Re-
481 trieved from `https://rmets.onlinelibrary.wiley.com/doi/full/10.1002/`
482 `qj.3414https://rmets.onlinelibrary.wiley.com/doi/abs/10.1002/`
483 `qj.3414https://rmets.onlinelibrary.wiley.com/doi/10.1002/qj.3414`
484 doi: 10.1002/qj.3414
485 Weisheimer, A., Decremer, D., MacLeod, D., O'Reilly, C., Stockdale, T. N., Johnson,
486 S., & Palmer, T. N. (2019). How confident are predictability estimates of the
487 winter north atlantic oscillation? *Quarterly Journal of the Royal Meteorological*
488 *Society*, *145*, 140–159.
489 Weisheimer, A., & Palmer, T. (2014). On the reliability of seasonal climate fore-
490 casts. *Journal of the Royal Society Interface*, *11*(96), 20131162.
491 Weisheimer, A., Schaller, N., O'Reilly, C., MacLeod, D. A., & Palmer, T. (2017,
492 jan). Atmospheric seasonal forecasts of the twentieth century: multi-decadal
493 variability in predictive skill of the winter North Atlantic Oscillation (NAO)
494 and their potential value for extreme event attribution. *Quarterly Journal of*
495 *the Royal Meteorological Society*, *143*(703), 917–926. doi: 10.1002/qj.2976
496 Weisheimer, C., A.; O'Reilly. (2020). *Initialised seasonal forecast of the 20th century.*
497 [dataset]. Centre for Environmental Data Analysis. Retrieved from `https://`
498 `catalogue.ceda.ac.uk/uuid/6e1c3df49f644a0f812818080bed5e45`

Figure1.png.

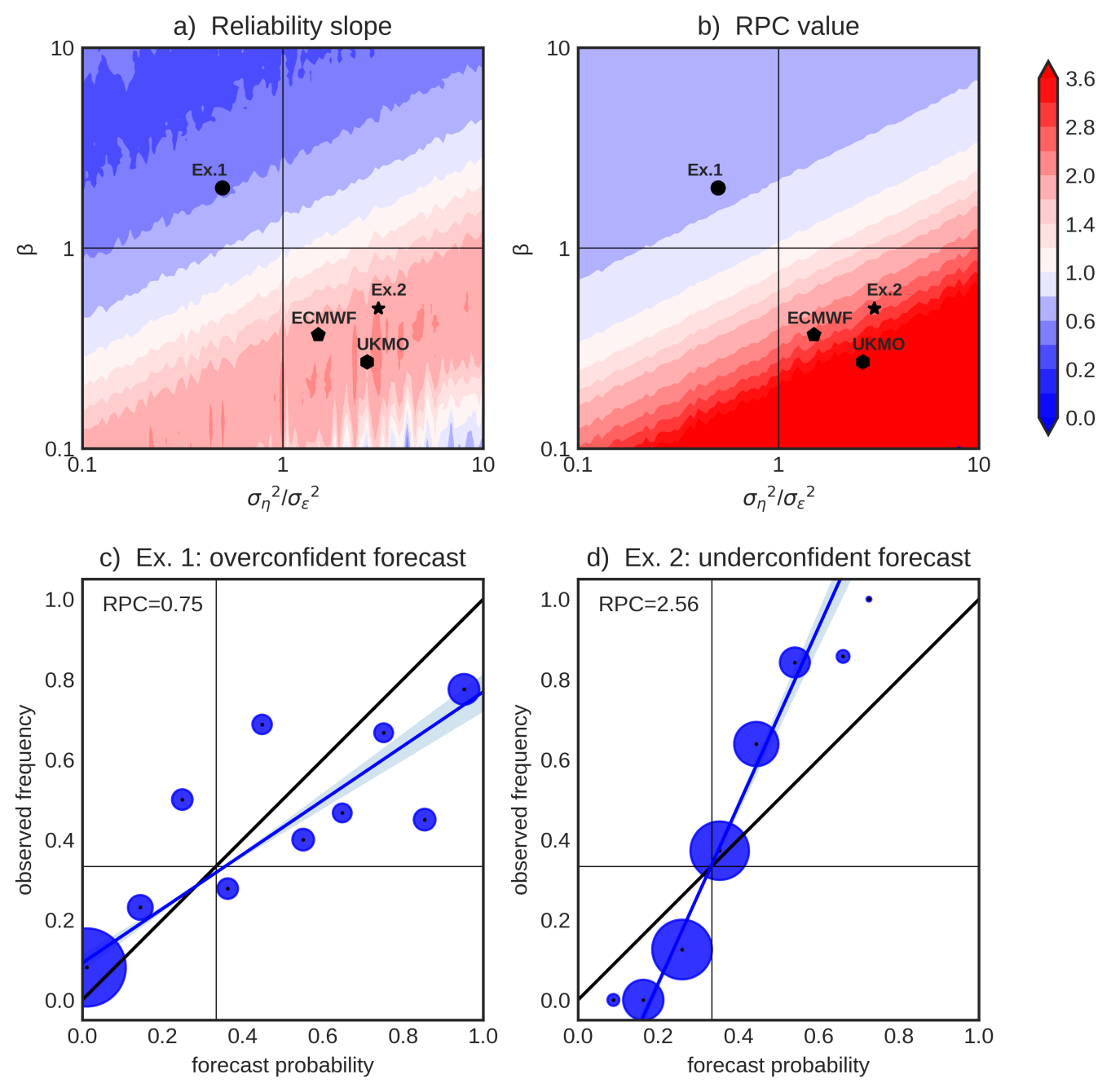
a) Reliability slope
b) RPC value
c) Ex. 1: overconfident forecast
d) Ex. 2: underconfident forecast
Ex.1
Ex.2
ECMWF
UKMO
β
$\sigma_\eta^2/\sigma_\varepsilon^2$
RPC=0.75
RPC=2.56
observed frequency
forecast probability
0.1
1
10
0.0
0.2
0.4
0.6
0.8
1.0
3.6
2.8
2.0
1.4
1.0
0.6
0.2
0.0

Figure2.png.

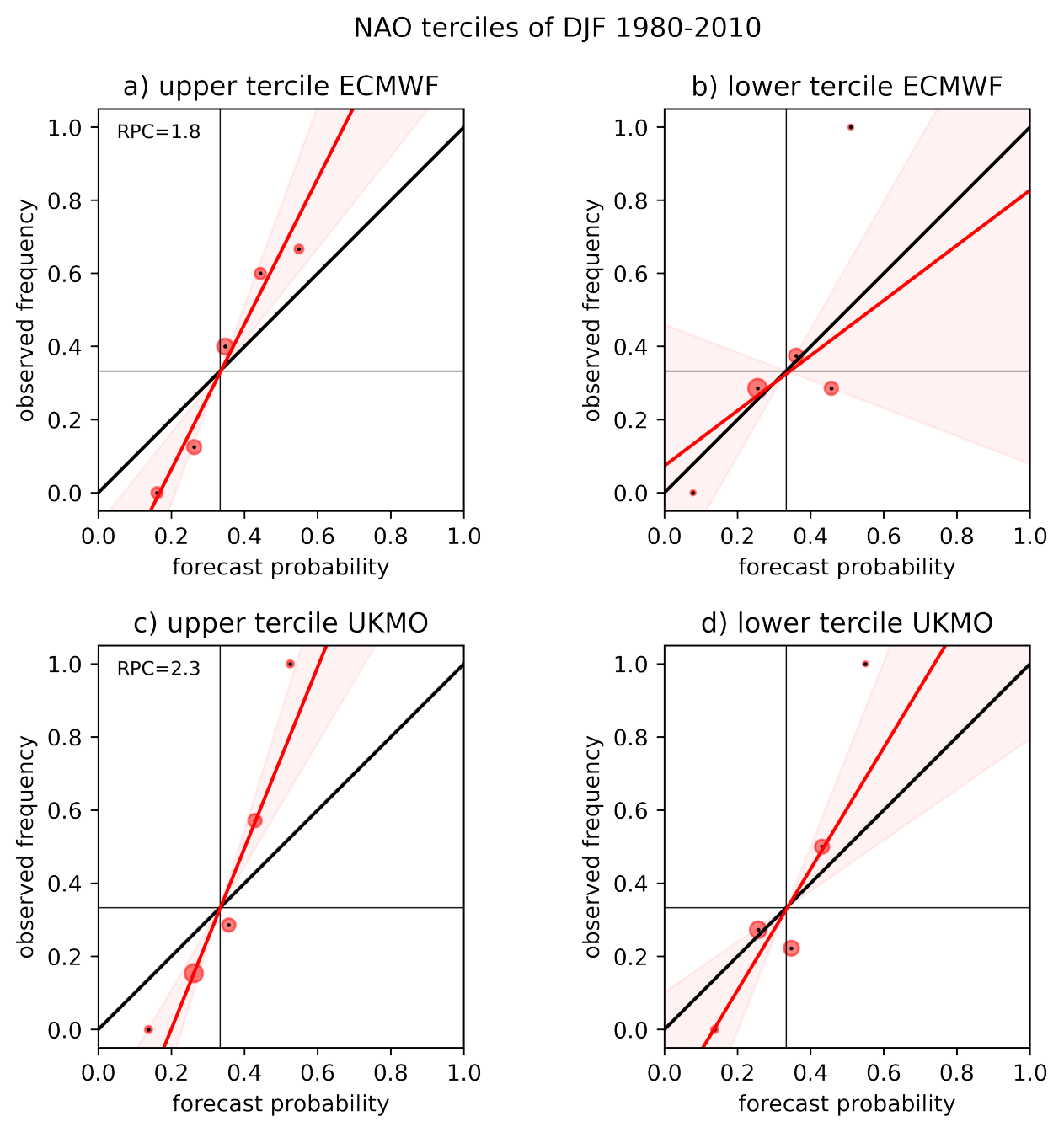
NAO terciles of DJF 1980-2010
a) upper tercile ECMWF
RPC=1.8
b) lower tercile ECMWF
c) upper tercile UKMO
RPC=2.3
d) lower tercile UKMO
observed frequency
forecast probability
0.0
0.2
0.4
0.6
0.8
1.0

Figure3.png.

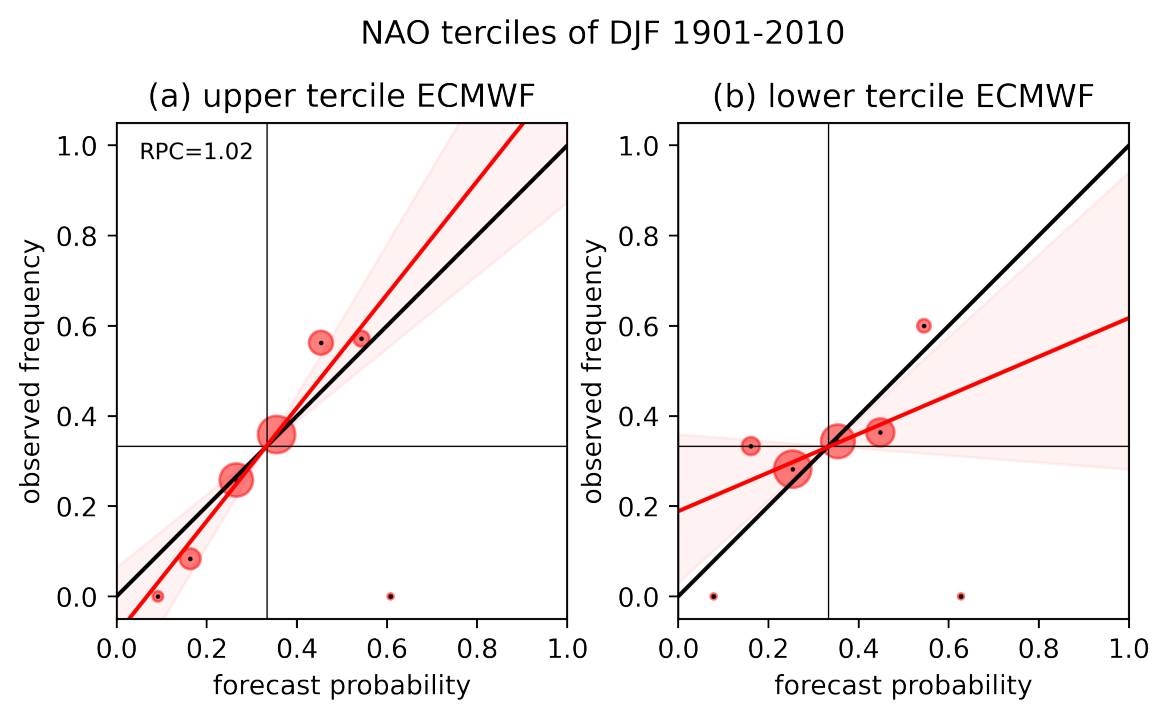
NAO terciles of DJF 1901-2010
(a) upper tercile ECMWF
(b) lower tercile ECMWF
RPC=1.02
observed frequency
forecast probability
0.0
0.2
0.4
0.6
0.8
1.0